Atmos. Chem. Phys. Discuss., 12, 6185–6204, 2012
www.atmos-chem-phys-discuss.net/12/6185/2012/
doi:10.5194/acpd-12-6185-2012

Atmospheric Chemistry and Physics Discussions

Trends, interannual and seasonal variations of tropospheric CO, C_2H_6 and HCN columns measured from ground-based FTIR at Lauder and Arrival Heights

G. Zeng[1], S. W. Wood[1,*], O. Morgenstern[1], N. B. Jones[2], J. Robinson[1], and D. Smale[1]

[1]National Institute of Water and Atmospheric Research, Lauder, New Zealand
[2]School of Chemistry, University of Wollongong, Wollongong, New South Wales, Australia
[*]now at: 1981 Omakau-Chatto Creek Road, Alexandra, New Zealand

Received: 29 November 2011 – Accepted: 19 February 2012 – Published: 27 February 2012

Correspondence to: G. Zeng (guang.zeng@niwa.co.nz)

Published by Copernicus Publications on behalf of the European Geosciences Union.

Abstract

We analyse the carbon monoxide (CO), ethane (C_2H_6) and hydrogen cyanide (HCN) partial columns (from the ground to 12 km) derived from measurements by ground-based solar Fourier Transform Spectroscopy at Lauder, New Zealand (45° S, 170° E) and at Arrival Heights, Antarctica (78° S, 167° E) from 1997 to 2009. Significant negative trends are calculated for all species at both locations: CO (-0.90 ± 0.31 % yr^{-1}) and C_2H_6 (-3.10 ± 1.07 % yr^{-1}) at Arrival Heights and CO (-0.87 ± 0.30 % yr^{-1}), C_2H_6 (-2.70 ± 0.94 % yr^{-1}) and HCN (-0.93 ± 0.32 % yr^{-1}) at Lauder. The uncertainties reflect the 95 % confidence limits. The dominant seasonal trends of CO and C_2H_6 at Lauder, and to a lesser degree at Arrival Heights, occur in austral spring when the correlations between CO and C_2H_6 and between CO and HCN maximize. Tropospheric columns of all three species are characterised by minima in March–June and maxima from August to November; this season is the southern-hemisphere tropical and subtropical biomass burning period. A tropospheric chemistry-climate model is used to simulate CO and C_2H_6 columns for the period of 1997–2009 using interannually varying biomass burning emissions; the model simulated tropospheric columns of CO and C_2H_6 compare well with the measured partial columns of both species. However, the model does not re-produce the significant negative trends of observed CO and C_2H_6 partial columns at both locations. Weak negative trends are calculated from model data. The model sensitivity calculations indicate that long-range transport of biomass burning emissions from Southern Africa and South America dominate the seasonal cycles of CO and C_2H_6 at both Lauder and Arrival Heights. Interannual variability of these compounds at both locations is largely triggered by variations in biomass burning emissions associated with large-scale El Nino Southern Oscillation and prolonged biomass burning events, e.g. the Australian bush fires.

ACPD
12, 6185–6204, 2012

1 Introduction

In the mid- and high latitudes of the Southern Hemisphere (SH), measurements of trace gases are sparse. Mid-infrared solar Fourier Transform Spectroscopic measurements (FTS) made by the National Institute of Water and Atmospheric Research at Lauder (45° S, 170° E, 370 m a.m.s.l.) and Arrival Heights (78° S, 167° E, 220 m a.m.s.l.) constitute the most comprehensive multi-year time series of trace gases in the Southern Hemisphere (http://www.ndsc.ncep.noaa.gov/). Measured species include not only those of significance to stratospheric ozone depletion, but also compounds crucial to understanding tropospheric pollution and transport (e.g., CO, C_2H_6, and HCN).

CO and C_2H_6 are among the most abundant ozone precursors in the troposphere and play a crucial role in controlling its oxidizing capacity. They are emitted primarily by anthropogenic sources and their main sinks in the troposphere are through reaction with the hydroxyl radical (OH) (e.g., Levy, 1971). The lifetimes of both species are around 50–60 days (Hough, 1991); hence they are influenced by vertical mixing and long-range transport. This makes them suitable indicators for transport of air pollutants. In the absence of major industrial sources of CO and C_2H_6 in the Southern Hemisphere, biomass burning emissions occurring in the southern tropics and subtropics are the main sources of both species (Watson et al., 1990; Fishman et al., 1991). For HCN, it is well established that biomass burning is the major source (Lobert et al., 1990); however, its sinks are not well quantified. It has a lifetime of around 2–4 months with the main sink suggested to be uptake by the ocean (e.g., Li et al., 2000). Therefore, measurements of these species made in the clean SH mid- to high latitudes are particularly useful in interpreting influences from the southern tropical and sub-tropical biomass burning through long-range transport.

Time series of CO, C_2H_6 and HCN columns at Lauder measured from mid-infrared FTS have been reported previously for various periods (e.g., Rinsland et al., 1998, 2002; Jones et al., 2001; de Laat et al., 2010). Rinsland et al. (1998) showed significant year-to-year variations in both CO and C_2H_6 partial columns (surface to 12 km)

ACPD
12, 6185–6204, 2012

measured at Lauder but the trends over the period 1993–1997 for both species are not significant. Rinsland et al. (2002) reported partial columns of the two species for the period of 1993–2000, as well as HCN for 1998–2000, at Lauder; again no significant long-term trends were found for CO and C_2H_6. However, Rinsland et al. (2002) reported a downward trend for HCN over this very short time period.

In this paper, we report extended time series of CO, C_2H_6, and HCN tropospheric columns from FTIR (Fourier Transform InfraRed) measurements at Lauder from 1997 to 2009, and CO and C_2H_6 columns at Arrival Heights for the same period that have not been presented in detail before. We calculate the trends of these species at both locations based on the 13-yr time-series and analyse their seasonal and interannual variability using a chemistry-climate model (CCM). In the following sections, we briefly describe the measurement technique, which has been extensively described before (e.g., Rinsland et al., 1998, 2002), and describe the CCM used for simulations and the comparison between modelled and observed time series of CO and C_2H_6 (we do not simulate HCN here as it requires more detailed information on its sources and sinks which is not the focus of this study). Furthermore we assess the main processes that contribute to seasonal and interannual variations of these species at the two stations that are representative of mid- and high latitudes of the Southern Hemisphere.

2 Description of measurements and model simulations

The measurement sites are both part of the Network for the Detection of Atmospheric Composition Change (NDACC) (http://www.ndsc.ncep.noaa.gov/). Measurements are possible only on clear days and, at Arrival Heights, there is a period of 4–5 months of polar night each year when solar measurements are not possible. The measurements were made at Arrival Heights with a Bruker model 120M Fourier Transform Spectrometer. The measurements at Lauder were initially made with a similar 120M but were changed to a 120HR Bruker model in September 2001. Both instrument models have the same maximum path difference of 257 cm, resulting in a spectral resolution of

ACPD
12, 6185–6204, 2012

0.0035 cm^{-1}. Mirror tracking systems were used to record direct sun spectra in the mid- infra-red (2–14 µm), using liquid nitrogen cooled detectors. The retrieval of trace gas information from these recorded spectra was performed using version 3.93 of the profile retrieval algorithm SFIT2 and is largely similar to that described by Rinsland et al. (1998, 2002).

The tropospheric chemistry-climate model, UM-CAM, is used to perform the simulations. The model was evaluated and used in a number of previous studies (e.g., Zeng et al., 2008, 2010), and is based on the UK Met Office Unified Model version 4.5 (atmosphere only) coupled with a detailed tropospheric chemistry scheme. It has 19 levels from surface to 4.6 hPa with 6 levels above 150 hPa. Its horizontal resolution is 3.75° by 2.5°. The model uses prescribed sea surface conditions following AMIP II (http://www-pcmdi.llnl.gov). The chemistry module includes gas phase reactions describing O_3-NO_x-VOC (volatile organic compounds) chemistry, dry and wet deposition, and tabulated photolysis rates as described by Zeng et al. (2008). Daily concentrations of NO_y above 50 hPa are prescribed using the output from a 2-D model (Law and Pyle, 1993). We also prescribe stratospheric ozone with a present-day ozone climatology that is for use in IPCC AR5 simulations (Cionni et al., 2011). The UM-CAM ozone fields are overwritten in the model domains above 50 hPa between 60° S–60° N and above 100 hPa poleward of ± 60°. As the model is not nudged towards observations, its day-to-day variations do not follow the observed weather. However, the seasonal-scale variability in the biomass burning emissions is captured, as well as major meteorological features such as ENSO which are present in the ocean-surface forcing.

We include surface emissions of NO, CO, C_2H_6, C_3H_8, HCHO, CH_3CHO, CH_3COCH_3 and isoprene, as well as NO emissions from aircraft in the model. Lightning-NO_x emissions are calculated online as a function of model-calculated cloud top height, as described by Zeng et al. (2008) and references therein. Methane mixing ratio is kept as a global constant (appropriate to year 2000 value, i.e. 1760 ppbv) to minimize the spin-up time of the simulations. Emissions of ozone precursors from

ACPD
12, 6185–6204, 2012

sources other than biomass burning have no year-to-year variations. The industrial sources of the species are adopted from the newly released emission scenarios for IPCC AR5 (Lamarque et al., 2010) for year 2000 conditions. For biomass burning emissions, we use the interannually varying Global Fire Emissions Database version 3 (GFED3) covering the years 1997 to 2009 (van der Werf et al., 2010). Total emissions of NMVOCs (non-methane volatile organic compounds) for both industrial and biomass burning sources are partitioned among the NMVOCs represented in the model to account for higher NMVOCs that are not included in the model. However the total global annual emissions for C_2H_6 are specified as 11.5 Tg yr^{-1} from industrial sources and around 5.2 Tg yr^{-1} from biomass burning (varying from year to year) in order to achieve more realistic atmospheric mixing ratios. We also scale the total isoprene emissions from 560 Tg yr^{-1} (Guenther et al., 1995), as used by Zeng et al. (2008) to 390 Tg yr^{-1} in this study; this produces a better match of modelled and measured CO and C_2H_6 columns, and is close to the estimates of Müller et al. (2008). There are large uncertainties in estimating global total annual isoprene emissions and the implementation of isoprene emissions in global models (Arneth et al., 2011).

3 Trends in tropospheric columns of CO, C_2H_6 and HCN between 1997 and 2009

Figure 1 shows measured instantaneous partial columns of CO, C_2H_6, and HCN at Lauder and CO and C_2H_6 at Arrival Heights in Antarctica (at both locations integrated between the surface and 12 km), displayed in black symbols (referred to in the following as "tropospheric columns"). The tropospheric columns of all 3 species show distinct seasonal cycles with low values during February–April and peaks over August–November at both locations. This indicates that in the absence of industrial sources in the Southern Hemisphere mid- to high latitudes, tropical biomass burning in the southern tropics is the main factor shaping the annual cycle (e.g., Rinsland et al., 1998; Matsueda et al., 1999). The annual cycle and variability of both C_2H_6 and CO tropospheric columns are larger at Lauder than at Arrival Heights, presumably due to the

ACPD
12, 6185–6204, 2012

larger transport times between the source regions and Arrival Heights, i.e. Antarctic air has experienced more mixing and photochemical removal than air above Lauder.

We form linear trends for each month separately. To account for different measurement densities, for every month covered by the time series, we perform a linear regression through the measurements taken during this month, and then evaluate the linear regression at the middle of the month to define one representative data point for each month. The multiannual trend is then calculated in a second step by linearly regressing through the representative mid-month values of each month. The result is referred to as the month-by-month linear regression. In a separate calculation, we also calculate multiannual trends by subtracting the mean annual cycle and calculating a linear trend from the remainder, following Rinsland et al. (2002). This analysis gives regression coefficients A_0 (a constant offset) and A_1, a linear trend term, and A_1/A_0 is the relative trend discussed below.

The multiannual relative trends and the uncertainties calculated for CO tropospheric columns are $-0.90 \pm 0.31\,\%\,yr^{-1}$ at Arrival Heights and $-0.87 \pm 0.30\,\%\,yr^{-1}$ at Lauder. For C_2H_6, the calculated trends are $-3.10 \pm 1.07\,\%\,yr^{-1}$ at Arrival Heights and $-2.70 \pm 0.93\,\%\,yr^{-1}$ at Lauder. Note the substantially larger relative trends of C_2H_6 than that of CO at both locations. Such larger trends of C_2H_6 relative to those of CO have also been detected at Northern Hemisphere locations (e.g., Angelbratt et al., 2011). Aydin et al. (2011) attribute the decline in global C_2H_6 levels since the 1980s to the decrease in C_2H_6 based fossil-fuel use in the Northern Hemisphere. They also speculate that atmospheric levels of chlorine atoms (Cl^*) might have increased which could potentially contribute significantly to the C_2H_6 decline. However, the magnitude of this sink is not well known. Measurements at Wollongong, Australia, also show negative trends of C_2H_6 (C. Paton-Walsh, personal communication, 2011). For C_2H_6, the main processes determining its abundance are its primary emission sources and its principal atmospheric sinks through the reaction with OH. Therefore understanding not only the changes in its primary sources but also the changes of OH in the past two decades is crucial to understanding its long-term trends. We speculate that in the absence of

ACPD
12, 6185–6204, 2012

industrial sources in the southern mid- to high latitudes, changes in OH could play an critical role in controlling trends in C_2H_6 in this clean environment. By comparison, sources of CO not only comprise emissions by primary sources; its chemical production also includes methane oxidation and degradation of higher hydrocarbons including C_2H_6. We note that relative trends in both CO and C_2H_6 are slightly larger at Arrival Heights than at Lauder. Although the relative trends are not significantly different at 95 % confidence level, this might indicate a systematic impact of transport or oxidizing capacity changes associated with climate change and/or stratospheric ozone changes. Considering expected further changes in both climate and stratospheric ozone, continued operation of observational platforms will be needed to detect such changes.

Rinsland et al. (2002) found no significant trends for either CO or C_2H_6 at Lauder between 1994 and 2000, but then these periods are very short for establishing significant trends. The 1997–1998 El Niño Southern Oscillation (ENSO) has influenced trends over that period, both directly by affecting transport and meteorology, and indirectly by causing major fires in Indonesia (Matsueda et al., 1999). However, Rinsland et al. (2002) report a large negative trend for HCN tropospheric columns at Lauder for 1998–2000 ($-8.06 \pm 1.06\,\%\,yr^{-1}$), presumably due to the 1997–1998 ENSO at the beginning of the time series. Here the calculated annual relative trend of HCN tropospheric columns at Lauder from 1998 to 2009 is $-0.93 \pm 0.32\,\%\,yr^{-1}$, which is comparable to the trends of CO tropospheric columns over this period.

Seasonal trends for the three species are shown in Fig. 2. The monthly trends from August to November are distinctly larger, in absolute terms, than at other months for both CO and C_2H_6 tropospheric columns at Lauder. This may indicate a downward trend of tropical biomass burning, although this is less apparent for HCN which is thought to also be produced by biomass burning, albeit with supposedly longer lifetime. At Arrival Heights, C_2H_6 and CO also exhibit largest negative trends over August to November. Note that the large negative trend for C_2H_6 tropospheric columns in February at Lauder is caused by persistent high levels recorded during February 1997, the beginning of the time series; this substantially affects the seasonal trend. Also note

ACPD
12, 6185–6204, 2012

that the slightly positive trend for CO tropospheric columns in February at Lauder, due to low values observed for February 1997. This is in contrast to the large amounts of C_2H_6 during this period. However, these anomalies do not play a significant role in determining annual trends for the whole period (1997–2009).

4 Seasonal and interannual variations

Figure 3 shows the correlation between the tropospheric columns of CO and C_2H_6, as well as CO and HCN in the four seasons for Lauder. The correlation coefficients vary with season for both sets of data and the largest correlation occurs during September–November when southern tropical biomass burning peaks (i.e. Pearson's correlation coefficients $r = 0.91$ for CO/C_2H_6 and $r = 0.88$ for CO/HCN). There are also considerably large correlations between CO and C_2H_6 during other seasons ($r = 0.70$–0.76). The correlation between CO and HCN is smallest during March–May ($r = 0.48$) when there is almost no southern sub-tropical biomass burning.

The seasonal and interannual variations of these species are compared with simulations from the UM-CAM CCM described in Sect. 2. Here we do not account for averaging kernels used in data retrievals (i.e. the difference in vertical resolutions and associated sensitivities) when comparing modelled and observed partial columns. The focus of the simulation is on characterizing the seasonal and interannual variations rather than improving the comparison between the modelled data and the observed data. Figure 4 shows the simulated daily mean CO and C_2H_6 tropospheric columns (integrated from the surface to ~150 hPa) between 1997 and 2009 at Lauder and Arrival Heights, respectively. The seasonal cycles are well reproduced by the model and clearly follow the cycle of the southern tropical biomass burning that peaks in austral spring (Hao and Liu, 1994). At Lauder, the observed CO and C_2H_6 partial columns both have larger variability in the observations than in the model. Note that individual and extreme events are generally not captured by the model, and the likely reasons for this include insufficiently variable emissions and excessive model diffusivity. At Arrival

ACPD
12, 6185–6204, 2012

Heights, however, the model data are much smoother owing to the longer transport distance from the emission source regions. The model underestimates the amplitude of the annual cycle of the species at Arrival Heights, especially for C_2H_6.

While the seasonal cycle and some of the interannual variability are well represented, the model simulations do not capture the significant observational trends for both CO and C_2H_6 tropospheric columns (Model shows weak negative trends for all species: −0.2 % in CO and −0.45 % in C_2H_6 at Arrival Heights and −0.3 % in CO and −0.65 % in C_2H_6 at Lauder). We speculate that a few factors might contribute to the lack of significant trends in our simulations: (1) the industrial sources used in the model have no temporal variations. This is however more of an issue in the Northern Hemisphere because most of these sources are from there, although they might affect SH through inter-hemispheric transport; (2) There may be trends in OH that the model does not capture (in particular, we do not consider stratospheric ozone changes over the simulation period, which might impact tropospheric ozone and its' oxidizing capacity; Zeng et al. (2010). However, these stratospheric changes were also generally small during this period.); (3) Biomass burning emissions might have trends that are not fully reflected in the database.

To examine the effect of biomass burning on the year-to-year variations of CO and C_2H_6 tropospheric columns, we contrast the model simulation described above (referred to as BBVAR) to a simulation that uses annually periodic biomass burning emissions, namely the GFED v3.0 dataset averaged over 1997 to 2009 (BBAVE). Figure 4, right panel, shows the daily mean percentage deviations of CO and C_2H_6 tropospheric columns due to variations in biomass burning (i.e. 100 × (BBVAR – BBAVE)/BBAVE) at Lauder and Arrival Heights. At both stations and for both species, the most substantial anomaly occurred during the 1997–1998 ENSO event which caused sustained burning in Indonesia. The anomalies at both locations are well correlated, indicating a persistent influence of transport of biomass burning pollutants over a large distance. For both CO and C_2H_6, the Lauder signal contains more short-lived spikes than the Arrival Heights series, suggesting either that the short-lived spikes disappear over the

ACPD
12, 6185–6204, 2012

few weeks of transport and mixing which separate the two sites, or possibly that there is an occasional influence of local emissions on the Lauder signal. Relative variations associated with C_2H_6 are larger than CO for both locations.

5 Impact of tropical biomass burning emissions

We also assess the impact of biomass burning emissions from different SH tropical and sub-tropical regions on tropospheric CO columns at mid- and high latitudes. A set of 4 sensitivity simulations is performed, consisting of repeating the BBVAR simulation but reducing by 50 % the biomass burning emissions from sub-equatorial Africa, South America, South-East Asia, and Australia, respectively. Figure 5 shows differences in the CO columns at Lauder and Arrival Heights in the 4 simulations, relative to BBVAR. The results indicate that African biomass burning dominates the background seasonality of SH CO columns, followed by emissions from South America. For most years, the contributions from South-East Asia and Australia are smaller in comparison, but they dominate the large peaks in 1998 and 2007, presumably as a result of the Indonesian fires in 1998 and Australian bush fires in late 2006 (the Great Divide Fires of 2006–2007 in Victoria), respectively. The 2006 Indonesian fires that contributed to elevated CO columns at Darwin (Paton-Walsh et al., 2010) does not have a significant influence on CO columns at Lauder and Arrival Heights from our sensitivity simulation. The simulation also indicates that the 2006 peak shown in Fig. 5 is caused by anomalously intensive burning in South America in late 2005.

6 Conclusions

We have analysed the Lauder and Arrival Heights CO, C_2H_6 and HCN tropospheric column time series from mid-infrared FTS measurements from 1997 to 2009. Statistically significant negative trends have been recorded for all three compounds at both

ACPD
12, 6185–6204, 2012

locations (ranging from −0.87 % to −3.1 % per year). These results supersede earlier results using data up to 2001, which did not have any significant trends. For CO and C_2H_6, relative trends at Arrival Heights are slightly larger than those at Lauder. C_2H_6 trends are significantly larger than CO trends at both locations. Maximum absolute trends occur in August to November for CO and C_2H_6 and June to September for HCN. The model reproduces well the year-to-year variability at both locations but underestimates the long-term trends. This may reflect either the absence of trends and interannual variability in the non-biomass burning emissions used in the model, or the omission of processes in the model that might affect trends, such as stratospheric ozone changes.

CO and C_2H_6, and CO and HCN tropospheric columns correlate highly, particularly during austral spring which is the primary SH tropical biomass burning season. All three species have similar seasonal variations peaking in austral spring. Stronger year-to-year variability is observed at Lauder, compared to Arrival Heights. This variability is largely caused by variations in SH tropical biomass burning. Model simulations indicate that biomass burning in Southern Africa and South America contributes substantially to the background seasonal variations of CO and C_2H_6 at Lauder and Arrival Heights. However, Indonesian fires triggered by the 1997–1998 ENSO and the prolonged 2006 Australian bush fires cause peaks in CO and C_2H_6 columns observed at Lauder for these periods. These peaks propagate efficiently to high latitudes.

Acknowledgements. This work is funded by the New Zealand Foundation for Research Science and Technology. We thank the UK Met Office for using the Unified Model and the support from NIWA HPC facility. We also thank Antarctica New Zealand for their logistic support and the University of Denver for installing the instrument at Arrival Heights. We acknowledge the use of the fire emissions from the Global Fire Emission Database version 3 (GFED3).

ACPD
12, 6185–6204, 2012

References

Angelbratt, J., Mellqvist, J., Simpson, D., Jonson, J. E., Blumenstock, T., Borsdorff, T., Duchatelet, P., Forster, F., Hase, F., Mahieu, E., De Mazière, M., Notholt, J., Petersen, A. K., Raffalski, U., Servais, C., Sussmann, R., Warneke, T., and Vigouroux, C.: Carbon monoxide (CO) and ethane (C_2H_6) trends from ground-based solar FTIR measurements at six European stations, comparison and sensitivity analysis with the EMEP model, Atmos. Chem. Phys., 11, 9253–9269, doi:10.5194/acp-11-9253-2011, 2011. 6191

Arneth, A., Schurgers, G., Lathiere, J., Duhl, T., Beerling, D. J., Hewitt, C. N., Martin, M., and Guenther, A.: Global terrestrial isoprene emission models: sensitivity to variability in climate and vegetation, Atmos. Chem. Phys., 11, 8037–8052, dio:10.5194/acp-11-8037-2011, 2011. 6190

Aydin, M., Verhulst, K. R., Saltzman, E. S., Battle, M. O., Montzka, S. A., Blake, D. R., Tang, Q., and Prather, M. J.: Recent decreases in fossil-fuel emissions of ethane and methane derived from firn air, Nature, 476, 198–201, 2011. 6191

Cionni, I., Eyring, V., Lamarque, J. F., Randel, W. J., Stevenson, D. S., Wu, F., Bodeker, G. E., Shepherd, T. G., Shindell, D. T., and Waugh, D. W.: Ozone database in support of CMIP5 simulations: results and corresponding radiative forcing, Atmos. Chem. Phys., 11, 11267–11292, doi:10.5194/acp-11-11267-2011, 2011. 6189

Fishman, J., Fakhruzzaman, K., Cros, B., and Nganga, D.: Identification of widespread pollution in the Southern Hemisphere deduced from satellite analyses, Science, 252(5013), 1693–1696, 1991. 6187

Guenther, A., Hewitt, C. N., Erickson, D., Fall, R., Geron, C., Graedel, T., Harley, P., Klinger, L., Lerdau, M., Mckay, W. A., Pierce, T., Scholes, B., Steinbrecher, R., Tallamraju, R., Taylor, J., and Zimmerman, P.: A global model of natural volatile organic compound emissions, J. Geophys. Res., 100(D5), 8873–8892, 1995. 6190

Hao, W. M. and Liu, M.-H.: Spatial and temporal distribution of tropical biomass burning, Global Biogeochem. Cycles, 8, 495–503, 1994. 6193

Hough, A. M.: Development of a two-dimensional global tropospheric model: model chemistry, J. Geophys. Res., 96(D4), 7325–7362, 1991. 6187

Jones, N. B., Rinsland, C. P., Liley, J. B., and Rosen, J.: Correlation of aerosol and carbon monoxide at 45° S: evidence of biomass burning emissions, Geophys. Res. Lett., 28(4), 709–712, 2001. 6187

ACPD
12, 6185–6204, 2012

de Laat, A. T. J., Gloudemans, A. M. S., Schrijver, H., Aben, I., Nagahama, Y., Suzuki, K., Mahieu, E., Jones, N. B., Paton-Walsh, C., Deutscher, N. M., Griffith, D. W. T., De Mazière, M., Mittermeier, R. L., Fast, H., Notholt, J., Palm, M., Hawat, T., Blumenstock, T., Hase, F., Schneider, M., Rinsland, C., Dzhola, A. V., Grechko, E. I., Poberovskii, A. M., Makarova, M. V., Mellqvist, J., Strandberg, A., Sussmann, R., Borsdorff, T., and Rettinger, M.: Validation of five years (2003–2007) of SCIAMACHY CO total column measurements using ground-based spectrometer observations, Atmos. Meas. Tech., 3, 1457–1471, doi:10.5194/amt-3-1457-2010, 2010. 6187

Lamarque, J.-F., Bond, T. C., Eyring, V., Granier, C., Heil, A., Klimont, Z., Lee, D., Liousse, C., Mieville, A., Owen, B., Schultz, M. G., Shindell, D., Smith, S. J., Stehfest, E., Van Aardenne, J., Cooper, O. R., Kainuma, M., Mahowald, N., McConnell, J. R., Naik, V., Riahi, K., and van Vuuren, D. P.: Historical (1850–2000) gridded anthropogenic and biomass burning emissions of reactive gases and aerosols: methodology and application, Atmos. Chem. Phys., 10, 7017–7039, doi:10.5194/acp-10-7017-2010, 2010. 6190

Law, C. S. and Pyle, J. A.: Modelling trace gas budgets in the troposphere: 1. ozone and odd nitrogen, J. Geophys. Res., 98, 18377–18400, 1993. 6189

Levy, H., II: Normal atmosphere: large radical and formaldehyde concentrations predicted, Science, 173, 141–143, 1971. 6187

Li, Q., Jacob, D. J., Bey, I., Yantosca, R. M., Zhao, Y., Kondo, Y., and Notholt, J.: Atmospheric Hydrogen Cyanide (HCN): biomass burning source, ocean sink?, Geophys. Res. Lett., 27(3), 357–360, 2000. 6187

Lobert, J. M., Scharffe, D. H., Hao, W. M., and Crutzeng, P. J.: Importance of biomass burning in the atmospheric budgets of nitrogen-containing gases, Nature, 346, 552–554, 1990. 6187

Matsueda, H., Inoue, H. Y., Ishii, M., Tsutsumi, Y.: Large injection of carbon monoxide into the upper troposphere due to intense biomass burning in 1997, J. Geophys. Res., 104(D21), 28867–28879, 1999. 6190, 6192

Müller, J.-F., Stavrakou, T., Wallens, S., De Smedt, I., Van Roozendael, M., Potosnak, M. J., Rinne, J., Munger, B., Goldstein, A., and Guenther, A. B.: Global isoprene emissions estimated using MEGAN, ECMWF analyses and a detailed canopy environment model, Atmos. Chem. Phys., 8, 1329–1341, doi:10.5194/acp-8-1329-2008, 2008. 6190

Paton-Walsh, C., Deutscher, N. M., Griffith, D. W. T., Forgan, B. W., Wilson, S. R., Jones, N. B., and Edwards, D. P.: Trace gas emissions from savannah fires in Northern Australia, J. Geophys. Res., 115, D16314, doi:10.1029/2009JD013309, 2010. 6195

ACPD
12, 6185–6204, 2012

Rinsland, C. P., Jones, N. B., Connor, B. J., Logan, J. A., Pougatchev, N. S., Goldman, A., Murcray, F. J., Stephen, M., Pine, A. S., Zander, R., Mahieu, E., and Demoulin, P.: Northern and Southern Hemisphere ground-based infrared spectroscopic measurements of tropospheric carbon monoxide and ethane, J. Geophys. Res., 103(D21), 28197–28217, 1998. 6187, 6188, 6189, 6190

Rinsland, C. P., Jones, N. B., Connor, B. J., Wood, S. W., Goldman, A., Stephen, T. M., Murcray, F. J., Chiou, L. S., Zander, R., and Mahieu, E.: Multiyear infrared solar spectroscopic measurements of HCN, CO, C_2H_6, and C_2H_2 tropospheric columns above Lauder, New Zealand (45° S latitude), J. Geophys. Res., 107(D14), 4185, doi:10.1029/2001JD001150, 2002. 6187, 6188, 6189, 6191, 6192

van der Werf, G. R., Randerson, J. T., Giglio, L., Collatz, G. J., Mu, M., Kasibhatla, P. S., Morton, D. C., DeFries, R. S., Jin, Y., and van Leeuwen, T. T.: Global fire emissions and the contribution of deforestation, savanna, forest, agricultural, and peat fires (1997–2009), Atmos. Chem. Phys., 10, 11707–11735, doi:10.5194/acp-10-11707-2010, 2010. 6190

Watson, C. E., Fishman, J., and Reichle, H. G. Jr.: The significance of biomass burning as a source of carbon monoxide and ozone in the Southern Hemisphere tropics: a satellite analysis, J. Geophys. Res., 95(D10), 16443–16450, 1990. 6187

Zeng, G., Pyle, J. A., and Young, P. J.: Impact of climate change on tropospheric ozone and its global budgets, Atmos. Chem. Phys., 8, 369–387, doi:10.5194/acp-8-369-2008, 2008. 6189, 6190

Zeng, G., Morgenstern, O., Braesicke, P., and Pyle, J. A.: Impact of stratospheric ozone recovery on tropospheric ozone and its budget, Geophys. Res. Lett., 37, L09805, doi:10.1029/2010GL042812, 2010.

6189, 6194

ACPD
12, 6185–6204, 2012

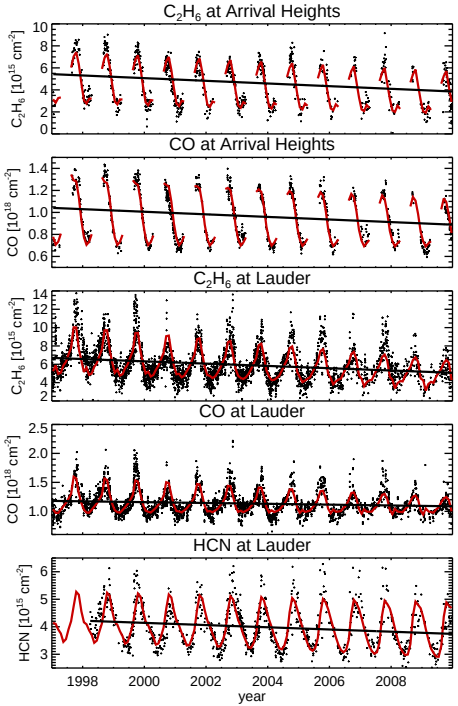

Fig. 1. Time series of CO, C_2H_6 and HCN tropospheric columns (molecules cm^{-2}) recorded at Lauder and Arrival Heights (black symbols), month-by-month linear regression (red line) and the multiannual linear trends (black line).

ACPD
12, 6185–6204, 2012

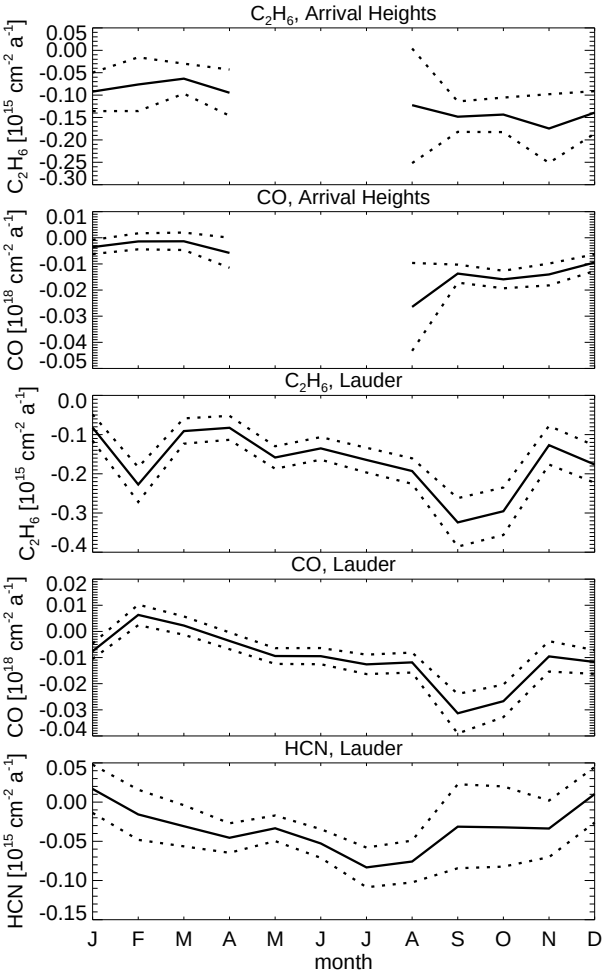

Fig. 2. Month-by-month trends (molecules cm^{-2} yr^{-1}) with associated 95 % confidence limits.

ACPD
12, 6185–6204, 2012

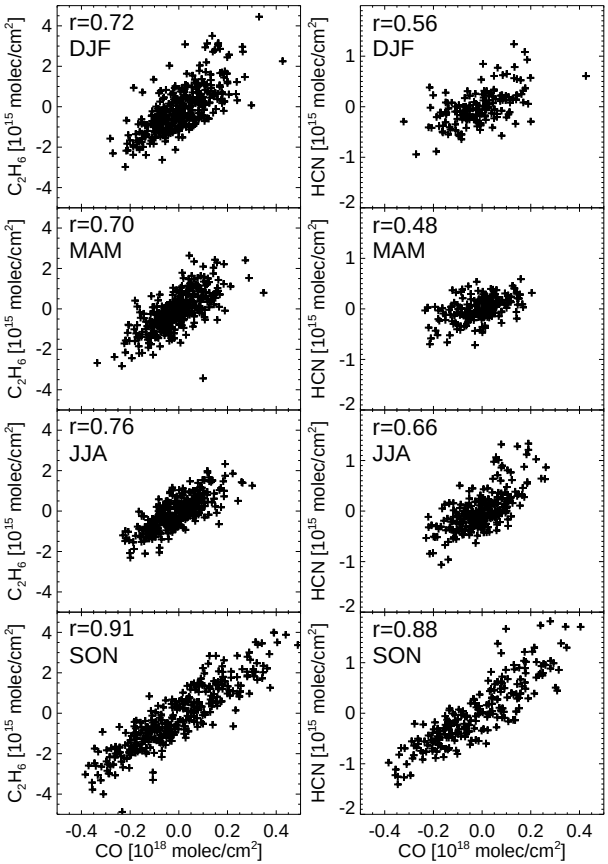

Fig. 3. Tracer-tracer correlative scatter plots for C_2H_6 and CO, and for HCN and CO, respectively, at Lauder for the four seasons. *r* indicates Pearson's correlation coefficient.

ACPD
12, 6185–6204, 2012

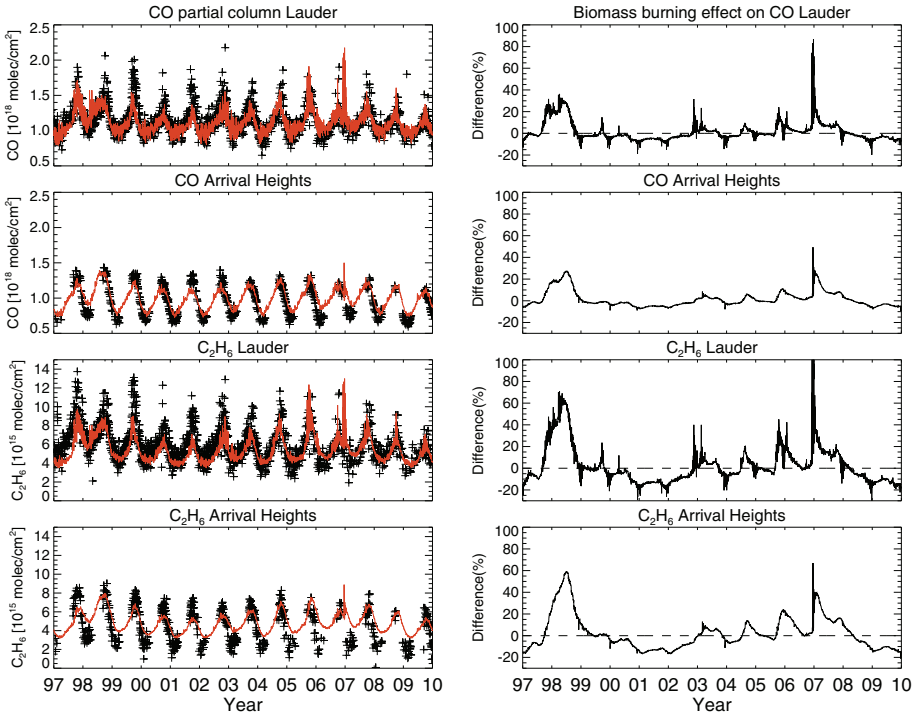

Fig. 4. Left panel: observed (black symbols) and modelled (red lines) CO and C_2H_6 tropospheric columns at Lauder and Arrival Heights. Right panel: percentage differences of corresponding CO and C_2H_6 columns simulated with interannually varying biomass burnings, relative to a simulation with annually periodic biomass burning emissions, taken as the average emissions over 1997–2009.

ACPD
12, 6185–6204, 2012

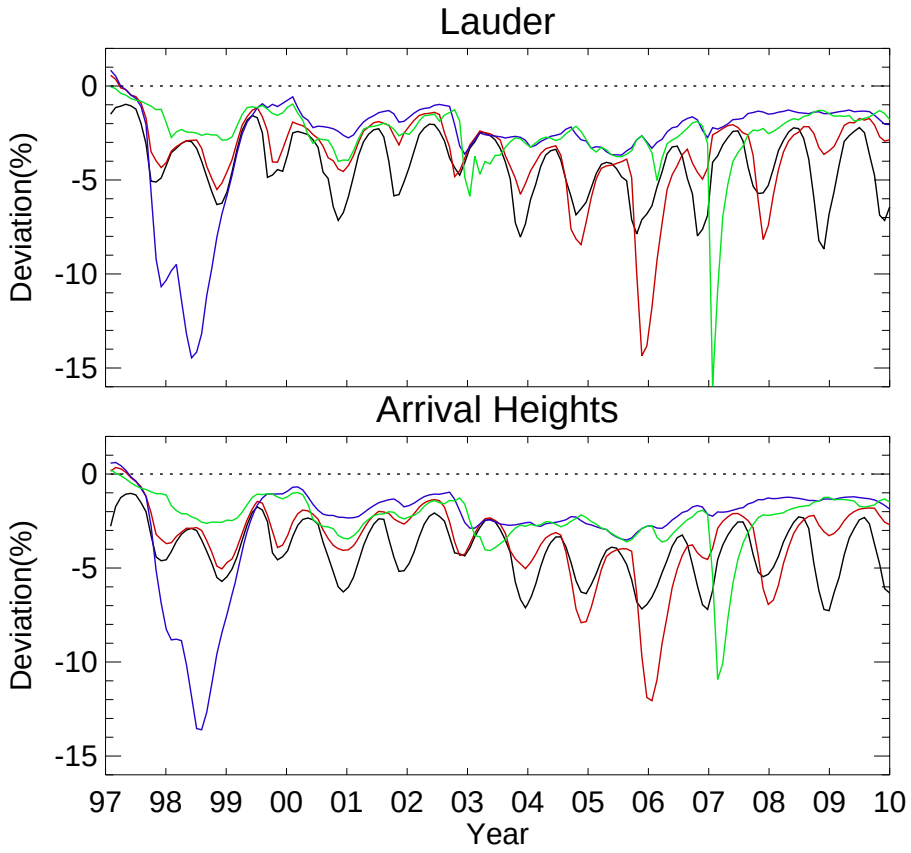

Fig. 5. Percentage differences of CO columns at Lauder and Arrival Heights, caused by 50 % reductions of biomass burnings from Southern Africa (blue), South America (red), South-East Asia (blue), and Australia (green).

ACPD
12, 6185–6204, 2012